Fermi National Accelerator Laboratory

FERMILAB-FN-629

Reduction of Tevatron and Main Ring Induced Backgrounds in the D0 Detector

J.M. Butler, D.S. Denisov, H.T. Diehl, A.I. Drozhdin, N.V. Mokhov and D.R. Wood

Fermi National Accelerator Laboratory
P.O. Box 500, Batavia, Illinois 60510

May 1995

Operated by Universities Research Association Inc. under Contract No. DE-AC02-76CHO3000 with the United States Department of Energy

Disclaimer

Reduction of Tevatron and Main Ring Induced Backgrounds in the DØ Detector

J. M. Butler, D. S. Denisov, H. T. Diehl, A. I. Drozhdin,
N. V. Mokhov, D. R. Wood

Fermi National Accelerator Laboratory

P.O. Box 500, Batavia, Illinois 60510

May 11, 1995

Abstract

Beam losses in the Fermilab Tevatron and Main Ring result in high occupancy in the drift chambers of the DØ detector. This causes increased muon trigger rates, complicates track reconstruction and causes aging of proportional drift chambers (PDTs). Veto methods in the Main Ring case reduce the integrated luminosity by about 20%. In April 1994 significant efforts were started in both the Accelerator and Research Divisions at Fermilab to explore the problem in detail and to find a way to reduce particle background levels in the DØ detector. Monte Carlo simulations were performed for beam loss in the Tevatron and Main Ring and for induced hadronic and electromagnetic showers in accelerator, shielding and detector components. As a result, an optimal shielding configuration was proposed and installed in the tunnel during August-September 1994 shutdown. In addition, the existing AØ scraper was replaced with a new one with two thin scattering targets. Measurements have confirmed a large effect from these improvements. Accelerator related backgrounds in the DØ detector have been significantly suppressed and now are much lower than those from the $p\overline{p}$ collision point.

Contents

1 Introduction

Experiments at high energy hadron colliders require special shielding against accelerator produced background particles. There are two main reasons which make this problem important: the detectors are situated directly in the accelerator tunnel and secondary particles produced by beam loss are of rather high energy, so they can punchthrough accelerator components and other equipment.

Since the begining of DØ operations two major sources of accelerator related backgrounds have been under study:

- Tevatron halo related backgrounds;
- Main Ring related backgrounds.

All background particles from accelerators originate in interactions of primary beam particles with residual gas and accelerator equipment. The improvements in beam quality, as well as appropriate shielding, can considerably reduce the backgrounds. The DØ experiment set up is presented in Figure 1 [1]. Proportional drift chambers (PDTs) of WAMUS and SAMUS muon detectors are affected by backgrounds more than other detectors. This is why we concentrate in this paper on improvement of the muon system background environment.

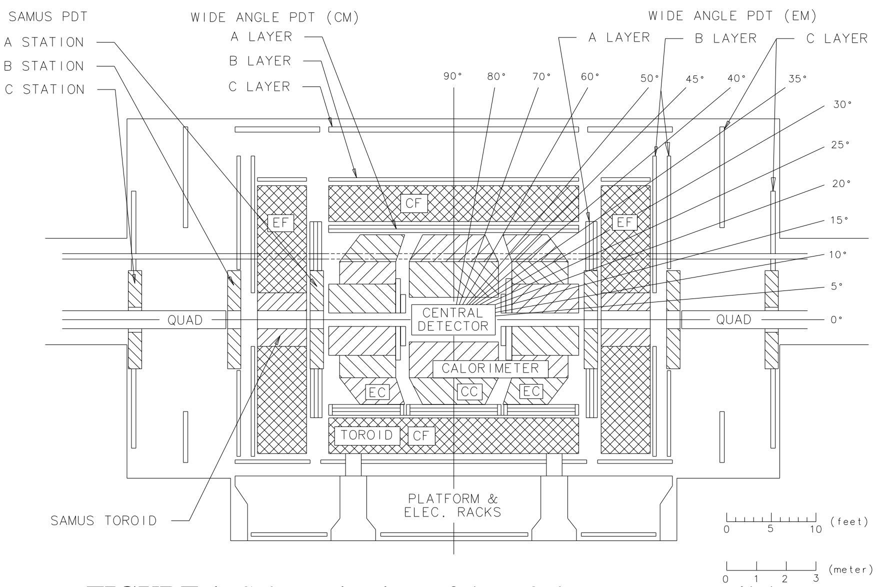

FIGURE 1. Schematic view of the D0 detector at Fermilab.

2 Backgrounds in the DØ detector

2.1 Tevatron Halo

Proton and antiproton beams can interact with accelerator equipment and residual gas during circulation in the Tevatron. Due to these interactions there is a halo of particles traveling simultaneousely with main bunches, but outside the beam envelope. As a result of beam halo interactions with limiting apertures, hadronic and electromagnetic showers are induced in accelerator and detector components. Products are detected in the DØ muon chambers: such particles pass through the outermost layer of a muon detector earlier than those from the collisions at the interaction point (IP). This time is equal to 63 ns in our case.

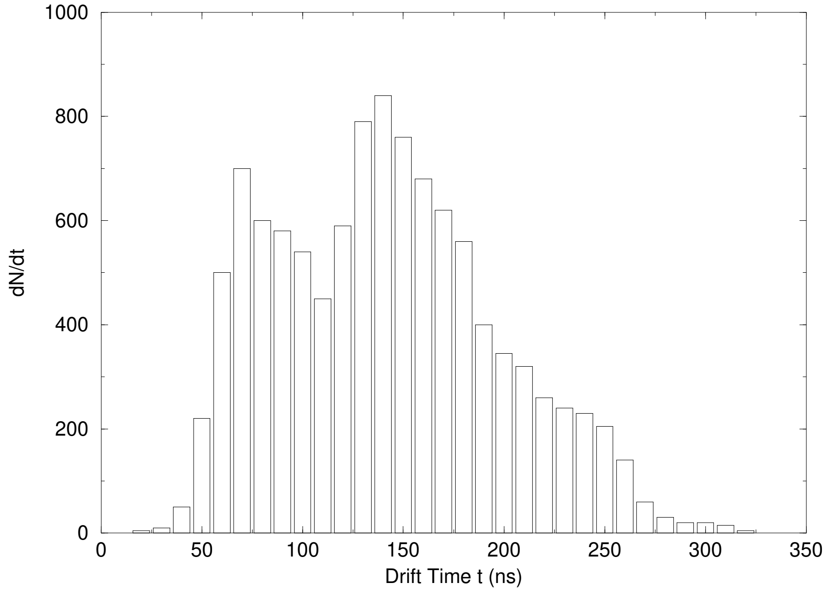

FIGURE 2. Drift time distribution (counts per 1 ns) for the outermost tube plane of the D0 detector in the "pre-shield" era.

Figure 2 shows typical drift time spectrum for a C-layer PDT in the "pre-shield" era. There were two peaks in the spectrum: at the beginning - from Tevatron halo, and later - from particles originated in $p\overline{p}$ collisions. The number of hits from halo particles for some stores was almost equal to the number of hits from particles originated from the collisions and collision remnants. Those hits produced the following problems for the data collection/analysis:

1. Substantially increased (by a factor of 2 to 10) muon trigger rates, which cause the DØ data aqusition system to saturate and also require prescales for muon triggers.

2. Background tracks found by muon track reconstruction program. These hits waste computer time as they are difficult to suppress and they lead to confusion in pattern recognition.

3. Additional source of aging of PDTs which is almost equal to the aging from particles that originate from the IP.

4. Saturation of the signals from the PDTs, causing inefficiency for the detection of real muons.

The beam halo induced fluxes are typically $\approx 3\times10^5\mathrm{m}^{-2}\mathrm{s}^{-1}$ at the luminosity of $10^{31}\mathrm{cm}^{-2}\mathrm{s}^{-1}$. The fluxes on the proton and antiproton sides of the detector are uncorrelated and typically the $\overline{p}$-halo is larger than the p-halo (normalized per appropriate beam intensities). Since the timing of the halo related particles differs by less than 100 ns from particles originated in the IP, it is impossible to suppress this background in the long drift time SAMUS/WAMUS PDTs.

2.2 Main Ring Halo

The Main Ring related background particles produce hits in the DØ muon PDTs. These hits are the origin of large currents drawn from the high voltage power supplies (HVPS). Figure 3 shows the HVPS current for one of the SAMUS drift tube plane of 3.3×3.3 m^2 area (see Fig. 1). One can see the spikes due to the Main Ring beam loss at injection of beam into the Main Ring and transition through the critical energy. Also, one sees increased current from HVPS each time the Main Ring beam passes the DØ collision hall. The pedestal is Tevatron related.

The estimated flux of particles in the SAMUS/WAMUS detectors during injection is $\approx 1.5\times10^6\mathrm{m}^{-2}\mathrm{s}^{-1}$. This background also produces energy deposition in the DØ liquid argon calorimeter, especially near the Main Ring beam pipe which passes directly through the calorimeter (see Fig. 1). $p\overline{p}$ events that occur during high losses in the Main Ring usually contain many more hits than events without the Main Ring activity, requiring the events be vetoed thus losing luminosity.

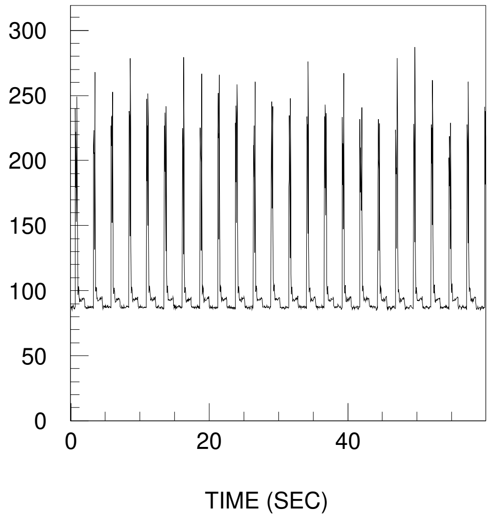

FIGURE 3. The HVPS current (μA) of one plane of the SAMUS drift tubes (C-layer) at the Tevatron luminosity of 8×10^{30} cm^{-2}s^{-1} and the Main Ring beam of 2×10^{12} protons.

Important features of the Main Ring related backgrounds are that, first, these are unstable in time (a factor of 2 or more variation depending upon accelerator conditions), and, second, the backgrounds at the downstream (with respect to proton direction) side are typically two times larger compared to those on the upstream side (without shielding wall on the downstream side). The current method of rejecting events with the Main Ring beam on is the following: veto data collection (for almost all triggers) during 0.40 sec at injection (so called a Main Ring beam loss signal) and veto data collection (for many triggers) for 2.6 μs each time the Main Ring beam passes the DØ collison hall. These vetoes almost completely reject events with hits from the Main Ring, but:

1. The Main Ring veto is a major source of the DØ dead time where approximetly 20% of the $p\overline{p}$ events are lost. This is the main source of difference between the CDF and DØ integrated luminosity.

2. The hits in PDTs lead to the "aging" – a degradation of the detector perfomance. The charge deposited on the PDT wires is proportional to the area under the curve in Fig. 3.

3. The Main Ring losses sometimes cause the HVPS trips due to overcurrent, which halts the data taking.

2.3 Experience with Shielding

In the design of the DØ detector special collimators were installed in the SAMUS toroids [2] to substantially decrease beam halo fluxes in the A-layer of the muon chambers and $p\overline{p}$-induced fluxes in the B and C-layers. Shielding on both sides of the CDF experimental hall was installed in 1992-1993 [3]. The CDF experience shows that concrete shielding walls in the accelerator tunnel considerably decrease accelerator related backgrounds and improve quality of the data collected.

3 Beam Loss and Induced Showers

3.1 Simulations

In our studies we assume the low-β Tevatron lattice [4] with the standard parameters for 900 GeV proton and antiproton beams. Two primary sources of beam loss in the Tevatron collider are considered: $p\overline{p}$ collisions at the BØ and DØ IPs, and beam halo interactions with the Tevatron scrapers. The events for the first term are simulated with the DTUJET93 code [5]. The beam halo interactions with the scrapers and the particle tracking through the lattice with a beam loss recording is done with the STRUCT code [6] with each lattice component taken into account. Beam loss induced hadronic and electromagnetic showers as well as the particle transport in the accelerator and detector components, in the Tevatron tunnel, the experimental hall including walls, and in the shielding, are simulated with the MARS code [7]. The energy thresholds are 1 MeV for muons and charged hadrons, 0.1 MeV for electrons and photons, and 0.5 eV for neutrons.

When simulating the beam induced showers, all the details of the 3-D geometry, materials and magnetic fields in the low-β quadrupoles Q2F (G = 125.562 T/m), Q3D (G = -124.004 T/m), Q4F (G= 126.000 T/m), in the Main Ring dipole magnets, in the tunnel and collision hall, and in the DØ detector muon system and the endcap calorimeter are included on both sides of the detector extended to 5 meter radius from the Tevatron beam line. Calculated values are the 3-D distributions of star density (density of inelastic hadron interactions) everywhere, and energy deposition, particle fluxes and energy spectra in the DØ PDTs (B and C-layers).

3.2 Beam Losses

The first analysis has shown that the accelerator related background in the DØ detector is due to beam loss in the inner triplet region, i.e. ±30 m from the interaction point. The main reason is that the β-function reaches its maximum in the final focus quadrupoles Q2 (horizontally) and Q3 (vertically) (Figure 4). So, there are two ways to mitigate the problem:

- minimization of the beam loss in the low-beta quads via increased Tevatron scraper efficiency;
- installation of the shielding walls at the Tevatron tunnel entrances at both ends of the DØ hall.

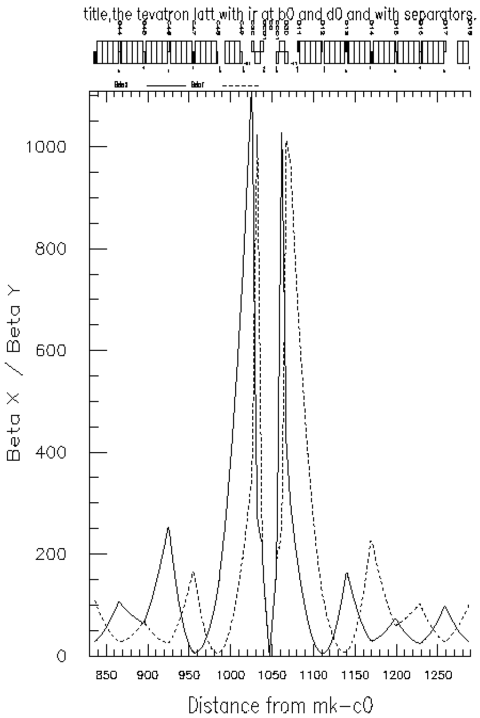

FIGURE 4. β-functions in the DØ interaction region as per N. Gelfand.

The first proposal [8] is based on the idea of using a thin scattering target to increase amplitude of the betatron oscillations of the halo particles and thus to increase their impact parameter on the scraper face on the next turns. It was shown [9, 10] that this results in a significant decrease of the outscattered proton yield and correspondingly of the total beam loss in the accelerator. The method would give an order of magnitude in beam loss reduction at future multi-TeV machines, but even at the Tevatron one could expect a noticeable effect. For the Tevatron, the minimal proposal was to replace the existing scraper at AØ with a new one with two 2.5-mm thick L-shaped tungsten targets with a 0.3 mm offset relative to the beam surface on the either end of the scraper. Calculated beam loss distributions in the Tevatron with and without scattering target at the AØ scraper are shown in Fig. 5 and 6, respectively. One can clearly see that expected beam losses in the DØ vicinity with a new scraper is about a factor of 2.5 lower. Such a replacement was done during the August-September 1994 shutdown. The rest of the paper deals with the second measure, the shielding wall design and study.

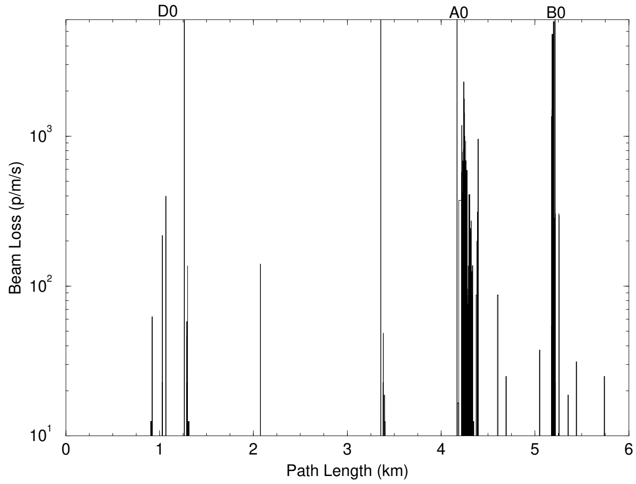

FIGURE 5. Beam loss rate in the Tevatron (baseline).

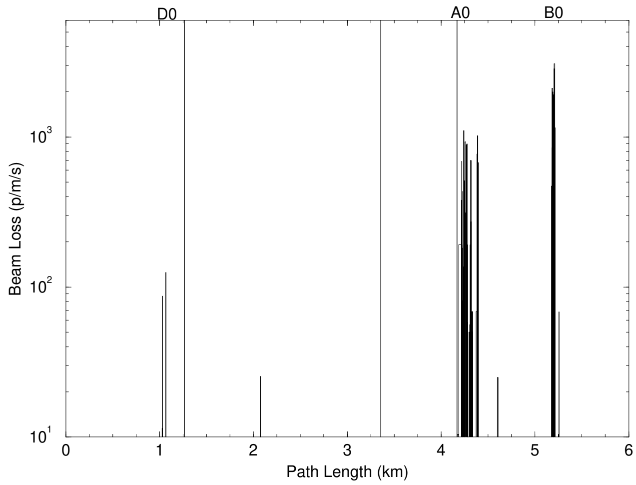

FIGURE 6. Beam loss rate in the Tevatron (with target at the AØ scraper).

4 Shielding Wall Efficiency

Longitudinal distribution of hadron inelastic events (star density) in the DØ low-β quadrupole beam pipe is presented in Fig. 7. The distribution, induced by halo particles, has a sharp maximum at the Q3 quad, naturally, just at the β-function related peak in the beam loss. Induced showers are peaked even closer to the IP, so the obvious way to intercept particle fluxes is to put a shielding wall as close to the collision hall as possible.

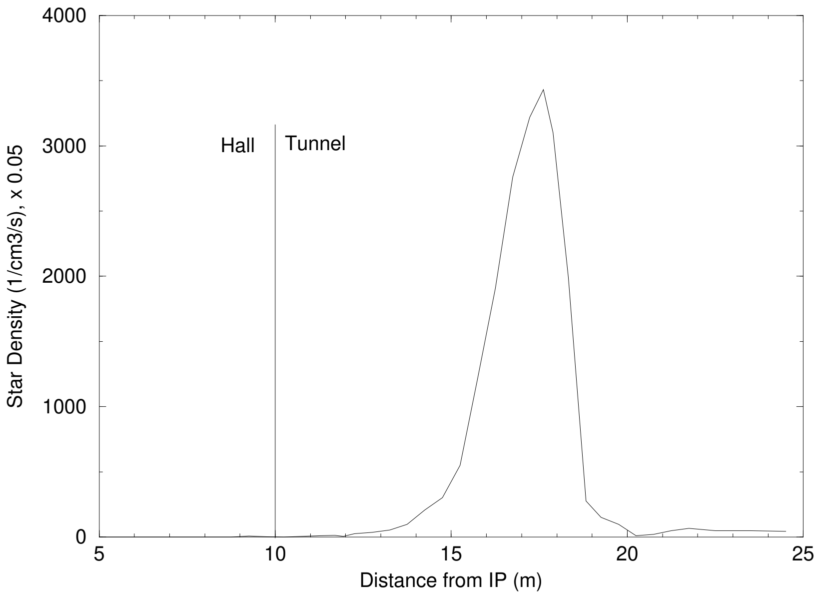

FIGURE 7. Intensity of the Tevatron halo induced nuclear interactions in the low-β quadrupole beam pipe.

Prior to our studies, a 1.5-m thick concrete wall was installed in the tunnel at about 19 m north (proton side) from the DØ interaction point. One can see from Fig. 7 that this wall was useless for intercepting particle fluxes from the beam loss peak. Of course, it absorbed a minor fraction of flux from the previous lattice section. Thus, our immediate proposal was to move existing wall closer to the hall, or to install another wall right at the tunnel-hall interface. It would also help to bring the Main Ring induced backgrounds down. In addition, to reduce background levels on the antiproton side, we proposed putting a similar shielding at the south end of the Tevatron tunnel entrance.

Results of the realistic multi-turn beam loss calculations were used for the Tevatron source term, while for the Main Ring we assumed a simplified model with longitudinally uniform beam loss in the magnets close to the hall. In calculations, we concentrated on the hottest regions of B- and C-layers of the DØ PDTs, namely on three radial intervals closest to the beam: 25–60 cm, 60–130 cm, and 130–230 cm. Although there is a variation in the azimuthal flux behaviour (particullary up-down asymmetry), most results were obtained, and analyzed, azimuthally averaged to improve statistics and to simplify analysis of the overall performance. Neutron spectrum at the C-layer (25≤r≤60cm) is shown in Fig. 8, with two well-known peaks, 0.8 MeV and 80–90 MeV, clearly seen. Fig. 9 shows hadron spectra at the B-plane (60≤r≤130cm). Particles with energy in excess of a few GeV are presented, but the main contribution to the hadron flux is due to low energy neutrons with E≤5 MeV.

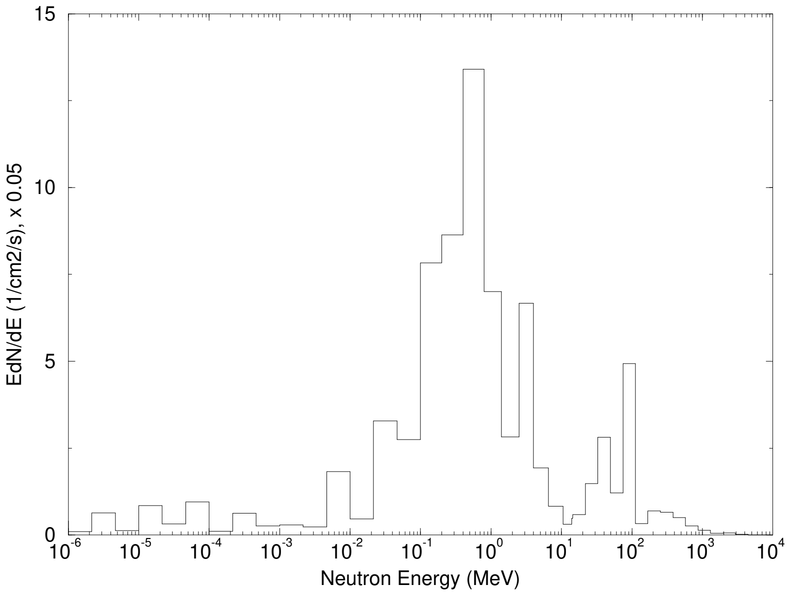

FIGURE 8. Neutron energy spectrum in the innermost region of the C-layer due to 0.9 TeV beam loss in the DØ low-β quadrupoles.

We found that charged hadrons bring typically about 1% to the total hadron flux in the WAMUS and SAMUS planes. At the same time, efficiency of the drift tubes for neutrons is only ≈0.001. So, the background rates and chamber gas aging are driven by the charged particles. This is especially true because of a dominant contribution from electromagnetic showers induced by π^0 decays.

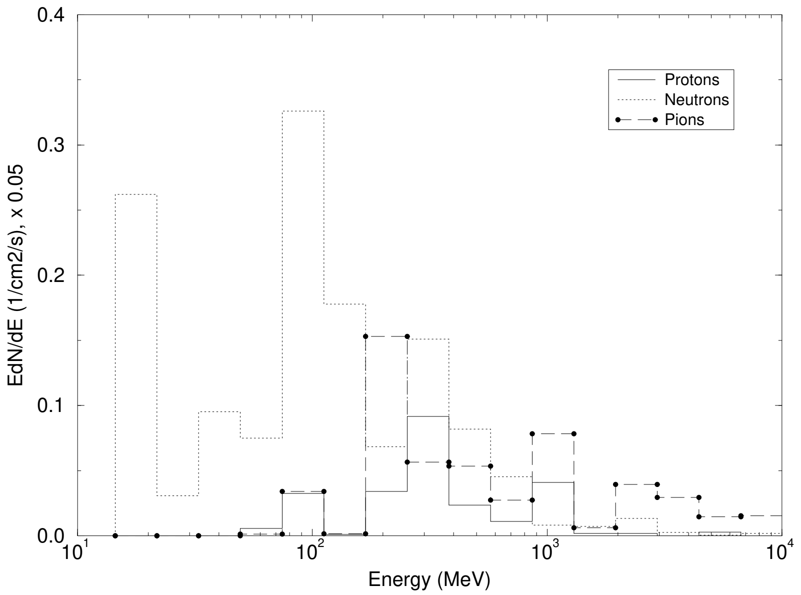

FIGURE 9. Proton, neutron and charged pion energy spectra at the B-layer due to 0.9 TeV beam loss in the DØ low-β quadrupoles.

Table 1 shows azimuthally averaged fluxes of neutrons, charged particles and photons at B- and C-layers for the proton and antiproton beam intensities which correspond to the luminosity of $10^{31}\mathrm{cm}^{-2}\mathrm{s}^{-1}$. With such a flux composition, the required ordinary concrete shielding wall thickness is about 1.8 m. There is almost no further reduction in the Tevatron induced flux at the DØ detector with increasing of the thickness above 1.8 m.

A few shielding configurations have been studied to find the one with highest efficiency while matching both the machine layout and the installation possibilities:

1. Baseline: "old" 1.5-m wall on the North (proton) side and no wall on the South (antiproton) side.

2. Baseline plus a new 1.8-m wall at the Tevatron tunnel entrances.

3. New 1.8-m walls at the Tevatron tunnel entrances.

4. Baseline plus reduced wall, 1.8-m thick at the bottom 60% of the height and 1.2-m thick the rest 40% of the height.

5. Configuration 4, but with a 30-cm gap around the Q4 quadrupole.

Table 1 : Neutron (n), charged particle ($h^{\pm}e^{\pm}$) and photon (γ) fluxes (cm^{-2}s^{-1}) for configuration 2 (ϕ-averaged). One R.M.S. statistical errors are 5–7% for neutrons with E$\leq$14 MeV, 15–20% for other hadrons, and 20–30% for electrons and photons. R$_1$=$n_{E\geq 14MeV}/n_{tot}$; R$_2$=$e^{\pm}/h^{\pm}e^{\pm}$.

Layer	r (cm)	n_{tot}	R$_1$	$h^{\pm}e^{\pm}$	R$_2$	γ
B	25–60	1.44	0.03	2.01	0.98	8.27
	60–130	1.20	0.03	0.28	0.91	1.20
	130–230	1.17	0.03	0.05	0.88	0.44
C	25–60	2.62	0.11	0.27	0.62	2.17
	60–130	1.78	0.08	0.09	0.62	1.16
	130–230	1.20	0.06	0.03	0.80	0.32

We define here a shielding efficiency as a ratio of the charged particle flux at the B- and C-layers in the baseline configuration to that in one of the new configurations. Tables 2 and 3 show this reduction factor at B- and C-layers for neutrons, charged particles and photons separately. Depending on the shielding configuration and on the location in the detector the background suppression can be as high as a factor of 12. On the average, for the charged component driving the detector response, the effect is not so high: about a factor of 5 for the C-plane and 3 for B-plane (Table 4). Results of this table will be compared with the measurements presented below.

Table 2 : Shielding efficiency (flux reduction) at the B-layer for neutrons (n), charged particles ($h^{\pm}e^{\pm}$) and photons (γ) in four shield configurations (ϕ-averaged).

r(cm)	Conf.	n_{tot}	$h^{\pm}e^{\pm}$	γ
25–60	2	7.42	1.49	1.46
	3	4.20	1.20	1.25
	4	5.77	1.38	1.43
	5	4.15	1.38	1.29
60–130	2	8.01	1.84	2.25
	3	5.68	1.36	1.95
	4	5.00	1.38	2.17
	5	4.83	1.77	2.04
130–230	2	7.68	3.74	5.84
	3	7.23	1.98	4.62
	4	7.46	3.07	4.84
	5	6.29	1.83	4.94

Table 3 : Shielding efficiency (flux reduction) at the C-layer for neutrons (n), charged particles ($h^{\pm}e^{\pm}$) and photons (γ) in four shield configurations (ϕ-averaged).

r(cm)	Conf.	n_{tot}	$h^{\pm}e^{\pm}$	γ
25–60	2	5.96	2.45	2.35
	3	3.51	2.29	2.13
	4	3.92	2.31	2.01
	5	2.73	1.13	1.06
60–130	2	8.64	7.12	5.88
	3	5.57	6.11	4.74
	4	6.50	6.37	4.34
	5	4.69	6.05	2.87
130–230	2	9.62	11.5	12.5
	3	8.86	10.8	12.2
	4	8.97	9.08	10.4
	5	6.39	5.95	10.3

If the new wall is thinner in the upper 40% part, the reduction factor is lower by about 15-20% for the Tevatron induced backgrounds and by almost 50-60% for the Main Ring backgrounds. The 30-cm gap around Q4 quadrupole increases fluxes at the detector by 35-77%, so we have proposed filling this gap with sand-bags with 10% addition of polybeads. Ideally, with the best shielding configuration and with the perfectly tuned new AØ scraper, the maximum background suppresion is expected to be as high as a factor of 8 at the North side and a factor of 12 at the South side.

Table 4 : Background reduction in the B- and C-layers at the North (proton) side related to the Tevatron (TEV) and Main Ring (MR) in four shield configurations. Charged particles, r- and ϕ-averaged.

Conf.	TEV (C)	TEV (B)	MR (C)
2	5.64	3.10	2.70
3	4.83	2.72	–
4	4.90	2.56	2.15
5	3.19	2.30	1.90

5 Shielding Installation

During the August-September 1994 Tevatron shutdown two concrete walls were installed on both sides of the DØ collision hall: the configuration 4 on the North (proton) side and the configuration 3 on the South (antiproton) side. The distance between collision hall and shielding walls is approximately 1 m — optimum according to above described simulations. Holes around the Main Ring and the Tevatron beam pipes were filled with sand-bags with 10% addition of polybeads.

6 Effect on Detector Performance

The WAMUS covers the muon detection region $|\eta| < 1.7$. The region $1.0 < |\eta| < 1.7$ tends to be sensitive to beam-related background. In order to study the effect of the shielding walls on these backgrounds, we monitored the currents of the power supplies which provide high voltage to the WAMUS PDTs. The fast histories of the currents are stored in the front ends of the supplies with a sampling period of 50 ms and a depth of 1 minute. The time structure of currents was used to separate the Main Ring induced component (spikes every 2 seconds) from the Tevatron induced component (baseline).

Fig. 10 shows a comparison of the Tevatron induced currents before and after the shield wall installation for some typical WAMUS chambers. The points show measured currents as a function of luminosity, where the stars were measured before the shield wall installation, and the circles were measured with the complete shield walls in place. The first plot is an example of current in the A-layer. These chambers are already well shielded by the iron toroids, and the addtional shieding of the walls has no apparent effect. The central B-layer and C-layer and the North and South B-layers are outside the iron, but are not located near the tunnel aperatures. They show a modest reduction of around 20% as a result of the shielding. The largest effect of the shielding is in the North and South C-layers, where the flux is reduced by a factor of 2 to 5, with some variation between North and South and up and down, since the proton and antiproton halos are different and the tunnel is not centered with respect to the beam axis. These B- and C-layer PDTs are the ones which have the largest currents and which suffer the most radiation damage, so the reduction of flux is most important in this region.

Note that flux which originates in the collisions should be proprotional to luminosity. Some comes directly from the interaction, and other comes from secondary scattering and showering of particles produced at large rapidity. The currents measured after the shield wall installation appear to vary approximately linearly with luminosity. Flux from halo will not necessarily track luminosity, and one can see large deviations from the linear relations in the pre-shielding points. As an additional cross check, we measured the currents during a store while the beams were separated at DØ after the shield walls were complete. With the beams separated, one measures only the flux from halo and no flux which originates from the interactions. The squares in Fig. 10 show the currents for separated beams. The luminosity just before and just after the beam separation was about 2.7×10^{30}. These show that virtually all of the remaining flux has its origin in the interaction.

The decrease of the Main Ring induced backgrounds for the WAMUS chambers is about a factor of 2. The effect is larger for the South side where no shielding wall existed before September 1994.

Effect of the shielding walls is even more dramatic for the SAMUS drift chambers situated in front of the accelerator tunnel. The decrease in a number of the beam halo hits (see Fig. 2) is 7 to 13 times for the B and C-layers. The A-layer is pretty well shielded by toroids. This reduction makes the number of halo related hits much less than that from $p\overline{p}$-collisions. This eliminates the Tevatron halo background problem almost completly. The Main Ring induced backgrounds were reduced by a factor of 2 for the North side and a factor of 3 for the South side, in a rather good agreement with the Monte Carlo predictions (Table 4).

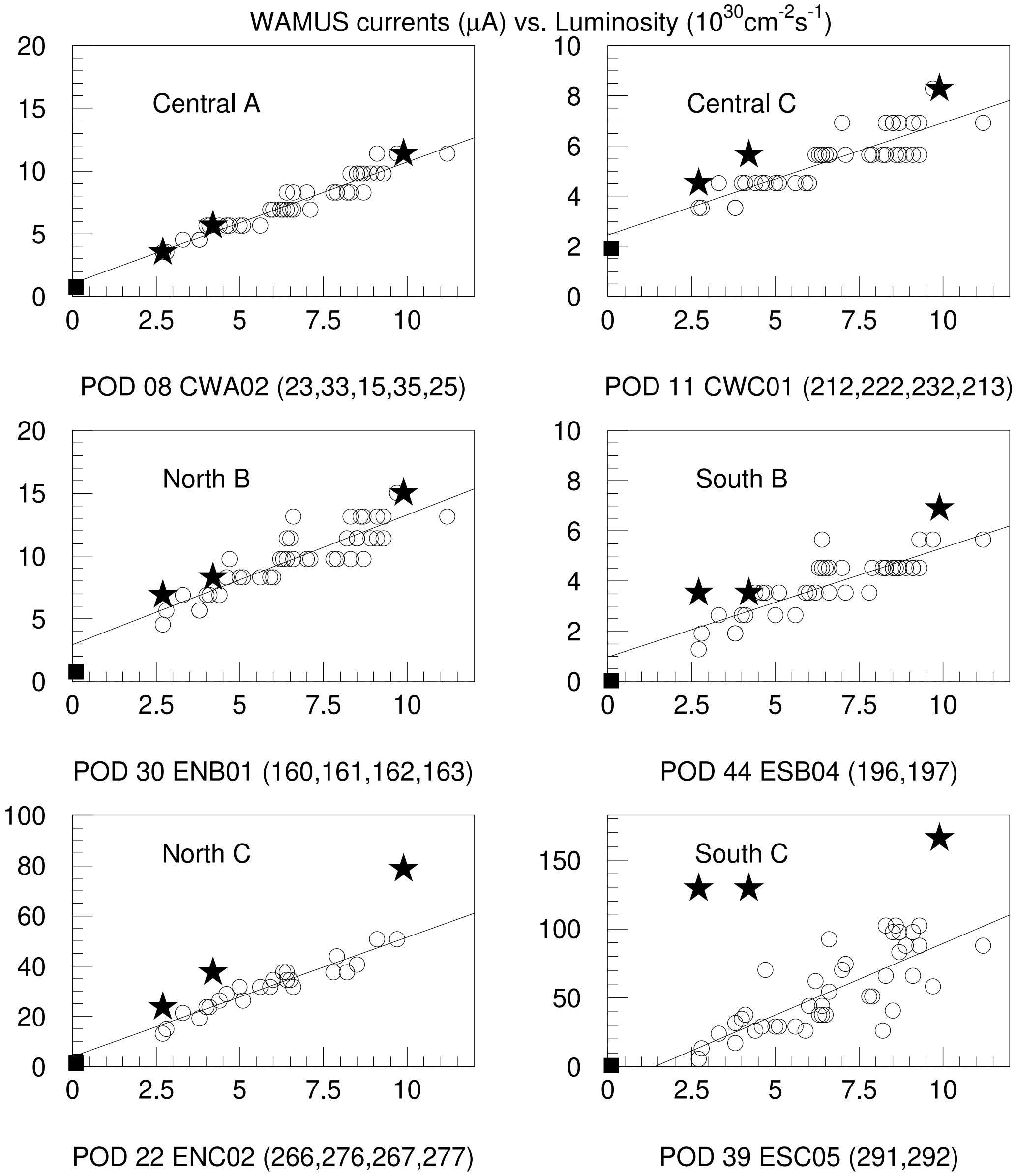

FIGURE 10. Measurements of HV currents in typical WAMUS chambers. The stars are measurements before the insallation of the shield walls, and the open circles are measurements after. The lines are linear fits to the post-shield wall points. The squares are measurements with beams separated in the post-shield configuration.

7 Conclusions

Accelerator induced background is an important problem for hadron collider experiments. Detailed calculations of the background sources in the DØ detector have lead to Tevatron scraper modifications and to a design for shielding walls on the both sides of the experimental hall. Relatively inexpensive concrete walls installed in the accelerator tunnel have decreased the Tevatron halo induced backgrounds up to a factor of 10 and the Main Ring induced backgrounds by about a factor of 2. Observed background reductions are in a good agreement with the Monte Carlo simulations. After installation of the shield walls, the Tevatron halo backgrounds became negligible compared to ones from the $p\overline{p}$-collisions. The Main Ring related backgrounds (PDT aging, HV trips) are now lower too.

8 Acknowledgements

The authors wish to thank R. Andrews, D. Augustine, P. Colestock, D. Finley, H. E. Fisk, N. Gelfand, M. May, H. Montgomery, J. Peoples, S. Pruss, L. Read, and M. Tartaglia for valuable discussions and support during a course of this work, and all staff of the AD/Mechanical Support Department for its effort in construction and installation of the shielding walls and new AØ scraper.

References

[1] “The D0 Detector”, *Nucl. Instruments and Methods*, **A338**, 185-253 (1994).

[2] N. V. Mokhov, “D0 SAMUS Background Studies”, *Fermilab D0 Note 721* (1988) and *Fermilab D0 Note 829* (1989).

[3] T. Fuess, and C. Wendt, “Shielding the FMU Rear Planes from Tevatron Losses”, *Fermilab CDF Note 1909* (1992).

[4] N. M. Gelfand, “Tevatron Lattice”, private communication (1994).

[5] P. Aurenche, F. Bopp, R. Engel, D. Pertermann, J. Ranft, and S. Roesler, “DTUJET93, Sampling Inelastic Proton-Proton and Proton-Antiproton Collisions According to the Two-Component Dual Parton Model”, *SI-93-3* (1994).

[6] I. Baishev, A. Drozhdin, and N. Mokhov, “STRUCT Program User’s Reference Manual”, *SSCL-MAN-0034* (1994).

[7] N. V. Mokhov, “The MARS Code System User’s Guide, Version 13(95)”, *Fermilab FN-628* (1995).

[8] A. I. Drozhdin, and N. V. Mokhov, “Increasing Tevatron Scrapers Efficiency”, Fermilab Accelerator Division Memo, July 1, 1994.

[9] M. A. Maslov, N. V. Mokhov, and I. A. Yazynin, “The SSC Beam Scraper System”, *SSCL-484* (1991)

[10] A. I. Drozhdin, N. V. Mokhov, R. Soundranayagam, and J. Tompkins, “Toward Design of the Collider Beam Collimation System”, *SSCL-Preprint-555* (1994).